



Event-triggered robust formation control of multi quadrotors for transmission line inspection

Tua Agustinus Tamba^{a,*}, Benedictus Christo Geroda Cinun^a, Yul Yunazwin Nazaruddin^b,
Muhammad Zakiyullah Romdlony^c, Bin Hu^d

^a Center for Control, Automation & Systems Engineering, Department of Electrical Engineering, Parahyangan Catholic University
Jl. Ciumbuleuit No. 94, Bandung, 40141, Indonesia

^b Department of Engineering Physics, Institut Teknologi Bandung
Jl. Ganesha No. 10, Bandung, 40132, Indonesia

^c School of Electrical Engineering, Telkom University
Jl. Telekomunikasi No. 1, Bandung, 40257, Indonesia

^d Department of Computer Engineering Technology & Science, University of Houston
4230 Martin Luther King Boulevard, Houston, TX 77204-4020, United States of America

Abstract

This paper proposes an event-triggered formation control scheme to manage the operation of multiple quadrotors in performing the inspection of a power transmission line. In particular, the problem of controlling such multi quadrotors to track the tower and/or cables of the transmission lines is considered. A multi-agent sliding mode control method is used for this purpose and is equipped with both a radial basis function neural network as an estimator of environmental wind disturbances, as well as an event-triggered scheduling scheme for the control execution framework. The proposed multi quadrotors control method is designed by considering the transmission tower/cable as the reference sliding surface. Simulation results are presented to illustrate the effectiveness of the proposed multi quadrotors control scheme when implemented in a case scenario of tracking the commonly-encountered shape of transmission cables. Simulation results are presented and show how the implementation of a position error-based event-triggered control enables all unmanned aerial vehicles (UAVs) to track the desired position and maintain a pre-determined formation. In particular, all UAVs can minimize the tracking error within 0.05 m after reaching the desired positions since the control signal is updated if the error reaches such an error bound.

Keywords: event-triggered control; formation control; multi-agent systems; radial basis function; sliding mode control.

I. Introduction

The Indonesian government is currently focusing on increasing the nation's electrification ratio/rate, especially in remote and rural areas. Various efforts have been made in this regard, which includes the development of new power generators as well as the

expansion of power transmission networks across the Indonesian archipelago. Based on the 2023 electrification statistical data from the state-owned company PT. PLN, it is known that Indonesia's overall electrification ratio has reached a value of 98.33 %, with a particular electrification rate of 99.76 % on Java Island [1]. These thus indicate the continuously

* Corresponding Author. ttamba@unpar.ac.id (T. A. Tamba)

<https://doi.org/10.55981/j.mev.2024.1106>

Received 28 November 2024; revised 16 December 2024; accepted 18 December 2024; available online 30 December 2024,
published 31 December 2024

2088-6985 / 2087-3379 ©2024 The Authors. Published by BRIN Publishing. MEV is Scopus indexed Journal and accredited as Sinta 1 Journal.
This is an open access article CC BY-NC-SA license (<https://creativecommons.org/licenses/by-nc-sa/4.0/>).

How to Cite: T. A. Tamba *et al.* "Event-triggered robust formation control of multi quadrotors for transmission line inspection," *Journal of Mechatronics, Electrical Power, and Vehicular Technology*, vol. 15, no. 2, pp. 197-207, Dec. 2024.

increasing size of the electric power source/generation and transmission networks in Indonesia that need to be monitored and inspected to ensure continuous provision of electric power.

One main challenge in maintaining/improving the availability and accessibility of electric power in remote and rural areas is with regard to the handling of various logistics that are required during the inspection and maintenance of the power transmission networks. The inspection of power transmission lines generally includes various tasks such as mapping and inspection of the transmission lines and their components, monitoring of vegetation conditions surrounding the transmission route, detection and assessment of potential icing along the transmission cables, and monitoring of potential damages due to extreme environmental conditions or natural disasters [2][3]. In many countries, including Indonesia, transmission line inspection activities are often done manually with the help of human field surveyors/technicians [4][5]. Such a manual inspection approach, however, has various disadvantages as it usually requires the deployment of a large number of human technicians/surveyors, takes long and lengthy inspection cycles and procedures, and offers low efficiency in terms of time, cost, and human/equipment resources [6][7]. Particularly for the case of power networks in rural and remote areas, these disadvantages are further exacerbated by the fact that the transmission lines have to go through extreme environmental conditions of steep mountains, deep rivers, or wild forests. In this regard, human surveyors/technicians often require significant additional time and deployment cycles to complete the required inspection process while at the same time needing to be extra careful in their work to ensure their safety [8][9]. These limitations of the conventional, human-dependent manual approach thus suggest the need for a more efficient and safer inspection method of power transmission lines/networks [10][11].

To address problems encountered by manual inspection processes, various kinds of unmanned robotics are used to save cost and time while ensuring safety and reliability [12]. In recent years, various studies and research have proposed the use of unmanned aerial vehicles (UAVs) to replace human surveyors/technicians for performing the inspection of power transmission lines [4][9]. Such a proposal was motivated by the realization that the use of UAVs for transmission line inspection offers various potential advantages, such as the possibility to explore extreme areas/routes, requires lower deployment time and cost, and reduces potential risks to operational safety [13]. Among others, prior research has examined the use of UAVs for the inspection of not only the transmission

line components (e.g., conductor, insulator, cable joint, and tower) but also the environment surrounding the transmission route (e.g., vegetation or wind profiles) [2][3]. Furthermore, various methods have been implemented to inspect power lines using UAVs, such as using cameras [14] or light detection and ranging (lidar) [15] as sensors that were mounted on the UAV to help with the inspection processes. However, most existing results remain limited to the case where only a single UAV is deployed at any time and requires the help/intervention of human operators in a teleoperation framework. In order to maximize the potential benefits that can be offered by UAVs' deployment/utilization, it is reasonable to argue that the present works need to be extended further to the case of multi-UAVs operation framework that can work autonomously to perform the inspection of electric power transmission lines.

This paper proposes an event-triggered formation control scheme to manage the operation of multi-UAVs in performing the inspection of a particular power transmission line. The specific task of inspection that is addressed in this paper is the problem of controlling multiple UAVs to track the tower and/or cable lines in the considered transmission network. Previous research regarding trajectory tracking purposes used the combination of integral sliding mode control (SMC) and backstepping-sliding mode control [16]. For this purpose, this paper proposes the use of a backstepping multi-agent SMC (B-SMC) method that is equipped with both an external disturbance estimator [17][18] as well as an event-based control execution scheduler [19][20][21]. The proposed SMC method is designed by considering the transmission tower/cable as the reference sliding surface. To account for and mitigate possible impacts of wind disturbances on UAVs' controlled movements, the development of the proposed B-SMC scheme also employs a radial basis function neural network (RBFNN) to provide an estimate of disturbance signals caused by external wind disturbances [22][23]. Finally, the execution of the designed control signal is implemented using an event-triggered control scheduling framework so as to achieve more efficient utilization of the available computation/communication resources in the proposed multi-quadrotor UAVs' operation scheme. Simulation results are also reported to illustrate the effectiveness of the proposed multi-UAVs control scheme when implemented in a case scenario of tracking a common shape of the transmission cable.

The remainder of this paper is structured as follows. Section II describes the dynamic model of each quadrotor UAV and states the problem of controlling

multi quadrotors for transmission line inspection applications. Furthermore, Section II also presents the proposed multi quadrotors cooperative control scheme, which features RBFNN-based disturbance estimation and event-triggered scheduling of control task execution. Simulation experiments for evaluating the performance of the proposed control scheme are presented in Section III. The paper is concluded with remarks and suggestions for future work in Section IV.

II. Materials and Methods

This section first determines the dynamic model and the formation scheme of the quadrotor UAV. Following this process, a B-SMC is used to make sure the quadrotor UAVs are able to reach the desired positions. Furthermore, external disturbances are estimated using RBFNN, and a position error-based event-triggered control is implemented for the position control. The setup for the simulation is presented at the end of this section.

A. Quadrotor UAV system

Consider the configuration dynamics of a quadrotor UAV in Cartesian frame $O - X - Y - Z$ as shown in Figure 1. The dynamics consist of position vector $x(t) = [x_1(t), x_2(t), x_3(t)]^T$ on the $X, Y,$ and Z axis, respectively, and orientation angle $\theta(t) = [\theta_1(t), \theta_2(t), \theta_3(t)]^T$ with respect to the $X, Y,$ and Z axis, respectively. The equations of motion (EoM) of the quadrotor UAV are given by a set of differential in equation (1) [23][24].

$$\begin{aligned}\ddot{x}_1 &= \frac{1}{m} [(\cos \theta_1 \sin \theta_2 \cos \theta_3 + \sin \theta_1 \sin \theta_3)F_j + \delta_1] \\ \ddot{x}_2 &= \frac{1}{m} [(\cos \theta_1 \sin \theta_2 \cos \theta_3 - \sin \theta_1 \sin \theta_3)F_j + \delta_2] \\ \ddot{x}_3 &= \frac{1}{m} (-mg + \cos \theta_1 \cos \theta_2 F_j + \delta_3) \\ \ddot{\theta}_1 &= \frac{1}{I_1} (\dot{\theta}_2 \dot{\theta}_3 (I_2 - I_3) + u_2) \\ \ddot{\theta}_2 &= \frac{1}{I_2} (\dot{\theta}_1 \dot{\theta}_3 (I_3 - I_1) + u_3) \\ \ddot{\theta}_3 &= \frac{1}{I_3} (\dot{\theta}_1 \dot{\theta}_2 (I_1 - I_2) + u_4)\end{aligned}\quad (1)$$

In equation (1), m is the quadrotor's mass, g is gravitational acceleration, (I_1, I_2, I_3) denote the quadrotor's moments of inertia with respect to the (X, Y, Z) axis, respectively, and $(\delta_1, \delta_2, \delta_3)$ are external disturbance signals due to wind or turbulent flows on the (X, Y, Z) axis, respectively.

The control input $u(t) = [F_j, u_2, u_3, u_4]^T$ driving the quadrotor's motion is defined as in equation (2), which consists of the thrust induced by the sum of forces F_j ($j = 1, \dots, 4$) produced by each propeller with

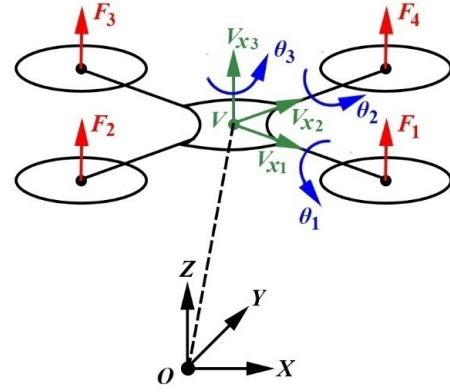


Figure 1. Schematic of a quadrotor UAV in Cartesian coordinate.

arm length L , and the total torques u_2, u_3 and u_4 on the (X, Y, Z) axis, respectively, that are induced by the combination of torques T_j produced by each propeller.

$$u(t) = \begin{bmatrix} F_j \\ u_2 \\ u_3 \\ u_4 \end{bmatrix} = \begin{bmatrix} F_1 + F_2 + F_3 + F_4 \\ L(F_4 - F_2) \\ L(F_3 - F_1) \\ T_2 + T_4 - T_1 - T_3 \end{bmatrix}\quad (2)$$

Define the vectors of state variables $x(t) = [x_i^k(t), \theta_i^k(t)]^T$, input $u(t) = [F_j, u_2, u_3, u_4]^T$, and disturbance signals $\xi(t) = [\delta(t), \mathbf{0}_{3 \times 1}]^T$ in which $\delta(t) = [\delta_1(t), \delta_2(t), \delta_3(t)]^T$ and $\mathbf{0}_{3 \times 1}$ is a column zero vector of dimension (3×1) . The dynamics of a quadrotor UAV under disturbances thus satisfy the EoM of the form equation (3).

$$\ddot{x}(t) = f(x(t), u(t)) + \frac{1}{m} \xi(t)\quad (3)$$

B. A leader-follower quadrotor formation scheme

To formulate the leader-follower formation scheme, let Q^* be a virtual reference leader with a position $x_i^* = [x_1^*, x_2^*, x_3^*]^T$ and heading angle θ_3^* . Consider the k -th follower quadrotor Q^k with position $x_i^k = [x_1^k, x_2^k, x_3^k]^T$ and heading angle θ_3^k (cf. Figure 2). Using vector and geometry analyses, the translational distance between the virtual leader and the k -th follower quadrotor may be defined as $\Delta_i^k \equiv [x_1^k - x_1^*, x_2^k - x_2^*, x_3^k - x_3^*]^T = [\Delta x_1^k, \Delta x_2^k, \Delta x_3^k]^T$. By taking into account the angle gap between the headings of the leader and followers, the desired position x_d^k of the k -th quadrotor for tracking the virtual leader quadrotor is defined as $\bar{x}_i^k = x_i^* + R_3(\theta_3^*) \Delta_i^k$, where R_3 denotes the rotation matrix with respect to the Z axis. Thus, if the k -th quadrotor in the group is required to track the position and heading angle of the virtual quadrotor, then the desired position \bar{x}_i^k and heading angle $\bar{\theta}_3^k$ it should maintain may be defined as in equation (4).

$$\bar{x}_i^k = x_i^* + R_3(\theta_3^*) \Delta_i^k, \quad \bar{\theta}_3^k = \theta_3^*\quad (4)$$

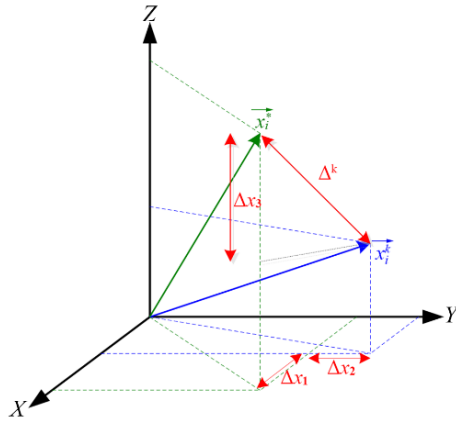


Figure 2. Schematic of the considered leader-follower scheme.

C. Wind disturbance estimation using RBFNN

This paper uses the RBFNN approach to estimate potential environmental disturbance signals $\delta(t)$ (e.g., wind forces) on model equation (1). A three (input, hidden, output) layers neural network is used to estimate disturbances on translation position and velocity signals of the k -th quadrotor. This is achieved using an activation/basis function as defined in equation (5).

$$\psi_j = \exp\left(-\frac{\|x^k - \mu_{1j}\|^2 + \|\dot{x}^k - \mu_{2j}\|^2}{b^2}\right) \quad (5)$$

where $j \in \{1, 2, \dots, n_j\}$ denotes the index of n_j neurons defined in the hidden layer of the designed neural network, μ_{1j} and μ_{2j} are the predetermined center point parameters for the assumed Gaussian distribution of disturbances in the position and velocity signals, respectively, and b is a parameter that controls the width of the Gaussian distribution function. Under such an activation function, the disturbances on the k -th quadrotor are assumed to take a form as in equation (6).

$$\delta^k = (\omega^k)^T \Psi^k + \zeta^k \quad (6)$$

in which ω^k denotes a weighting matrix, Ψ^k is the output of the hidden layer of the k -th quadrotor, while ζ^k is some approximation errors. Using the RBFNN scheme, an approximation of disturbance signals can be computed according to equation (7).

$$\tilde{\delta}^k = (\tilde{\omega}^k)^T \Psi^k \quad (7)$$

In equation (7), the trained estimate of the weighting matrix $\tilde{\omega}^k$ is computed according to the rule in equation (8).

$$\tilde{\omega}^k = \alpha \left(\Psi^k (\mathcal{S}_x^k)^T - \nu \|\mathcal{S}_x^k\| \tilde{\omega}^k \right) \quad (8)$$

where \mathcal{S}_x^k is the sliding surface which will be defined in the next section. Furthermore, for the update of the weighting matrix, the momentum factor is denoted as q

where $0 < q < 1$. Note that such an RBFNN estimation scheme has been implemented in various computational software tools such as MATLAB [25].

D. Position and attitude controller design

1) Position Control Design

To design the position controller, consider the k -th quadrotor's translation dynamics that are defined by the first three rows of equation (3) as equation (9).

$$\ddot{x}_i^k(t) = f_l(x(t), u_1^k(t)) + \delta(t), \quad \text{for } i, l = 1, 2, 3 \quad (9)$$

Taking into account its desired position \bar{x}_i^k as in equation (4), define $e^k(t) \equiv x_i^k(t) - \bar{x}_i^k(t)$ as the quadrotor's position error. To ensure such a position error goes to zero, this paper utilizes the B-SMC approach. In particular, the control signal is designed to ensure the k -th quadrotor's position trajectories converge to and remain on a sliding surface defined in the following equation (10).

$$\mathcal{S}_x^k = \alpha e^k(t) + \dot{e}^k(t) \quad (10)$$

where $\dot{e}^k(t) \equiv \dot{x}_i^k(t) - \dot{\bar{x}}_i^k(t)$ denotes the quadrotor's linear velocity error and $\alpha > 0$ is a constant gain. Note in the sliding surface equation (10) that the leader's reference velocity $\dot{x}_i^*(t)$ needs to be defined in such a way that it guarantees the stability of the closed-loop system. In this paper, we use a reference leader velocity for the k -th quadrotor of the equation (11).

$$\dot{x}_i^*(t) = \dot{\bar{x}}_i^k - e^k(t) \quad (11)$$

Using a quadratic Lyapunov function $V_e = \frac{1}{2} \beta (e^k(t))^T e^k(t)$ in which $\beta > 0$ is a constant parameter, it can be shown that $\dot{V}_e \leq -\beta |e^k(t)|^2 < 0$ is satisfied, thereby showing that the chosen leader's reference velocity in equation (11) for the sliding surface in equation (10) guarantees the closed loop system remains Lyapunov stable.

The position control signal $u_1(t)$ for the k -th quadrotor is constructed into two parts, i.e. $u_1^k(t) = u_{1,1}^k(t) + u_{1,2}^k(t)$. The first control signal $u_{1,1}^k(t)$ is intended to lead/force the position trajectory towards the sliding surface, while the second one $u_{1,2}^k(t)$ is used to maintain the position trajectory to remain on the sliding surface. In this paper, the following control signals are used for each of such purposes, defined in equation (12).

$$\begin{aligned} u_{1,1}^k(t) &= -c_{1,1} \text{sgn}(\mathcal{S}_x^k) - c_{1,2} \mathcal{S}_x^k \\ u_{1,2}^k(t) &= \dot{x}_i^*(t) - \alpha (\dot{x}_i^k - \dot{\bar{x}}_i^k) - \tilde{\delta}(t) \end{aligned} \quad (12)$$

in which $(c_{1,1}, c_{1,2}) > 0$ are constant design parameters, while $\text{sgn}(\mathcal{S})$ denotes a piecewise continuous function as defined in equation (13).

$$\text{sgn}(\mathcal{S}) = \begin{cases} 1, & \text{if } \mathcal{S} > \epsilon \\ -1, & \text{if } \mathcal{S} < -\epsilon \\ \frac{1}{\epsilon}\mathcal{S}, & \text{otherwise} \end{cases} \quad (13)$$

where ϵ is a predefined positive constant with $0 < \epsilon < 1$. Under the control signal equation (12), one may examine the position error dynamics of the k -th quadrotor as defined by the sliding surface equation (10) using a quadratic Lyapunov function $V_S = \frac{1}{2}(\mathcal{S}_x^k)^T \mathcal{S}_x^k$. Taking the time derivative of V_S with respect to the position trajectories in equation (9) and under the control signal $u_1^k(t) = u_{1,1}^k(t) + u_{1,2}^k(t)$ in equation (12), it can be shown that $\dot{S}_p = -c_{1,1}(\mathcal{S}_x^k)^T \text{sgn}(\mathcal{S}_x^k) - c_{1,2}\|\mathcal{S}_x^k\|^2 \leq 0$ holds and thereby guaranteeing Lyapunov stability of the position control system.

The output $u_1^k(t) = [u_{1,x}^k, u_{1,y}^k, u_{1,z}^k]$ of the position controller serves as an input to the converter block, which is then used to determine the desired roll and pitch angles $\bar{\theta}_1(t)$ and $\bar{\theta}_2(t)$, respectively, and the total force F_j as defined as equation (14).

$$\begin{aligned} \bar{\theta}_2^k &= \arctan\left(\frac{u_{1,x}^k \cos \bar{\theta}_3^k + u_{1,y}^k \sin \bar{\theta}_3^k}{u_{1,z}^k + g}\right) \\ \bar{\theta}_1^k &= \arctan\left(\cos \bar{\theta}_2^k \frac{u_{1,x}^k \sin \bar{\theta}_3^k + u_{1,y}^k \sin \bar{\theta}_3^k}{u_{1,z}^k + g}\right) \\ F_j &= \frac{u_{1,z}^k + g}{\cos \bar{\theta}_1^k \cos \bar{\theta}_2^k} \end{aligned} \quad (14)$$

2) Attitude Controller

The construction of the attitude controller considers the quadrotor's rotational dynamics, which are defined by the last three rows of equation (3) as equation (15).

$$\ddot{\theta}_i^k(t) = f_i(x(t), u_r(t)), \text{ for } i = 1, 2, 3 \text{ and } l = i + 3 \quad (15)$$

where $u_r(t) = [u_2, u_3, u_4]^T$. Moreover, the controller is designed so as to ensure that the attitude error $\varepsilon^k(t) = \theta_i^k(t) - \bar{\theta}_i(t)$ between the virtual leader's attitude and the actual attitude of the k -th quadrotor goes to zero. For this case, the B-SMC scheme is also used with a sliding surface function as defined in equation (16).

$$\mathcal{S}_\theta^k = \gamma \varepsilon^k(t) + \dot{\varepsilon}^k(t) \quad (16)$$

in which $\gamma > 0$ is a designed parameter and $\dot{\varepsilon}^k(t) \equiv \dot{\theta}_i^k(t) - \dot{\bar{\theta}}_i(t)$ denotes the k -th quadrotor's angular velocity error. In this paper, the desired angular velocity of the k -th quadrotor is set to be of the form $\dot{\bar{\theta}}_i(t) = \theta_i^* - \varepsilon_i^k(t)$, in which θ_i^* is the virtual leader quadrotor's angular velocity.

Based on the sliding surface defined in equation (16), the attitude controller $u_r^k(\theta_i) = u_{r,1}^k(t) + u_{r,2}^k(t)$ is also constructed in two

parts: the first control $u_{r,1}^k(t)$ is to lead the altitude towards the sliding surface and the second control $u_{r,2}^k(t)$ is to maintain the attitude trajectory to remain on the sliding surface. For the roll angle, the used attitude controller $u_2^k(t)$ components are equation (17).

$$u_{2,1}^k(\theta_1) = -I_1 \left(c_{2,1} \text{sgn}(\mathcal{S}_{\theta_1}^k) + c_{2,2} \mathcal{S}_{\theta_1}^k \right) \quad (17)$$

$$u_{2,2}^k(\theta_1) = \left(\dot{\theta}_1^* - \gamma_1 (\dot{\theta}_1 - \dot{\bar{\theta}}_1) \right) I_1 - \dot{\theta}_2^k \dot{\theta}_3^k (I_2 - I_3)$$

where $c_{r,i} > 0$ are designed parameters. For the pitch angle case, the attitude controller $u_3^k(t)$'s components can be constructed in a similar manner as the following form equation (18).

$$u_{3,1}^k(\theta_2) = -I_2 \left(c_{3,1} \text{sgn}(\mathcal{S}_{\theta_2}^k) + c_{3,2} \mathcal{S}_{\theta_2}^k \right) \quad (18)$$

$$u_{3,2}^k(\theta_2) = \left(\dot{\theta}_2^* - \gamma_2 (\dot{\theta}_2 - \dot{\bar{\theta}}_2) \right) I_2 - \dot{\theta}_1^k \dot{\theta}_3^k (I_3 - I_1)$$

Finally, the attitude controller $u_4^k(t)$ components for the yaw angle are also defined similarly to obtain the form equation (19).

$$u_{4,1}^k(\theta_3) = -I_3 \left(c_{4,1} \text{sgn}(\mathcal{S}_{\theta_3}^k) + c_{4,2} \mathcal{S}_{\theta_3}^k \right) \quad (19)$$

$$u_{4,2}^k(\theta_3) = \left(\dot{\theta}_3^* - \gamma_3 (\dot{\theta}_3 - \dot{\bar{\theta}}_3) \right) I_3 - \dot{\theta}_1^k \dot{\theta}_2^k (I_1 - I_2)$$

E. Event-triggered control execution scheme

To formulate an event-triggered control scheme, recall that the k -th quadrotor's position control is $u_1^k(t) = u_{1,1}^k(t) + u_{1,2}^k(t)$ with elements that are defined as in equation (12). An event-triggered control scheme is proposed based on the position error between the desired position and the current position of the k -th quadrotor. In the proposed event-triggered control scheme, the event-triggered state error is defined as equation (20).

$$e_i^k(t) \equiv \bar{x}_i^k(t) - x_i^k(t) \quad (20)$$

which calculates the position difference between the k -th quadrotor and the desired one at time t .

In this paper, the event-triggered scheme is used for the position controller as illustrated in Figure 3. In this figure, the event-triggered block receives the current position error and the current control signal generated by the position controller. For the control execution scheme proposed in this paper, the control signal is updated if the following condition is violated as equation (21).

$$|e_i^k(t)| \leq e_{th} \quad (21)$$

where e_{th} is the event-triggered constant threshold value. While the commonly used threshold function for event-triggered scheme is e^{-kt} , this paper opts for a constant threshold value for simplicity. Therefore, the

Table 1.

Model parameters for individual quadrotor, the controller parameters, and the RBFNN network parameters.

Individual quadrotor parameters		Controller parameters		RBFNN parameters	
Parameter	Values	Parameter	Values	Parameter	Values
m	1	β	3	n_j	50
g	9.8	α	2	a	0.2
I_1	0.01	c_1	2	b	20
I_2	0.01	λ	5	v	0.2
I_3	0.02	γ	5	q	0.3
		c_2	2	μ_1 and μ_2	$[\mu_x, \mu_y, \mu_z]^T$
		c_3	2		
		c_4	2		

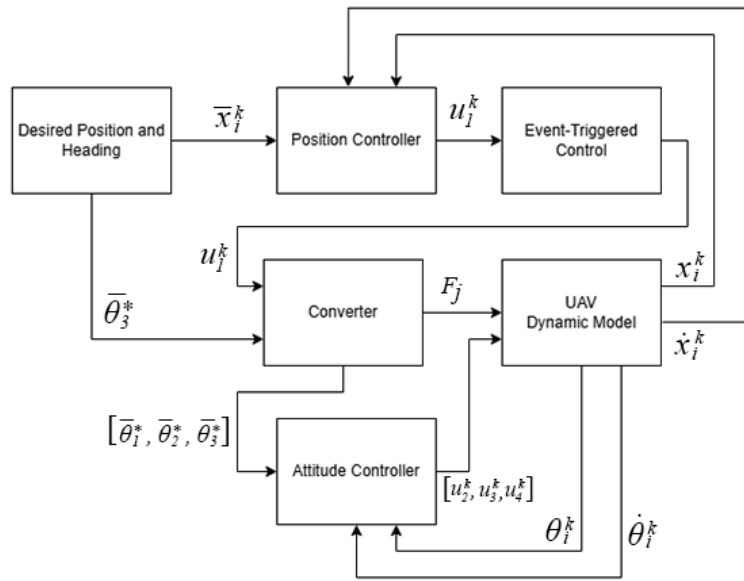


Figure 3. Schematic of UAV control diagram.

control signal will not be updated until the position error value reaches a predetermined threshold value. In this regard, the event-triggered control update scheme is determined according to the logic in equation (22).

$$\begin{cases} u_1^k(t) = u_1^k(t_s^k) \\ t_{s+1}^k := \inf \{t > t_s^k \mid (|e_i^k(t)| \leq e_{th}) \vee (t - t_s^k > T)\} \end{cases} \quad (22)$$

F. Simulation setup

For the simulation scenario, each quadrotor is required to start and maintain a predetermined distance from the virtual leader during its flight. The initial positions and required distances are as follows: UAV 1: $x^1 = [1, 0, 0]^T$; $\Delta^1 = [-2, -2, 2]^T$, UAV 2: $x^2 = [2, 0, 0]^T$; $\Delta^2 = [2, -2, 2]^T$, UAV 3: $x^3 = [1, 1, 0]^T$; $\Delta^3 = [2, 2, -2]^T$, UAV 4: $x^4 = [2, 1, 0]^T$; $\Delta^4 = [-2, 2, -2]^T$.

The reference trajectory is defined into three segments. The first segment starts from the ground to the top of the first tower. The second one defines a

parabolic curve of transmission cables between two supporting towers. The third segment defines a path from the top to the bottom of the second tower. The trajectory was constructed following the time progression of the simulation using the pseudocode in Algorithm 1.

Algorithm 1 Reference Trajectory Generation

- 1: **if** $t < 6.5$ **then**
- 2: $xd = 0, yd = 0, zd = t, \psi d = -45$
- 3: **else if** $6.5 < t < 26.5$ **then**
- 4: $xd = t - 6.5, yd = t - 6.5,$
 $zd = 0.015(t - 16.5)^2, \psi d = -45$
- 5: **else**
- 6: $xd = 20, yd = 20, zd = 6.5 - (t - 26.5),$
 $\psi d = -45$
- 7: **end**

Table 1 shows the model parameters implemented in the proposed RBFNN-based B-SMC control scheme, the controller parameters, and the neural network

model parameters. For the RBFNN parameters, the μ_x , μ_y and μ_z values are generated by the following MATLAB syntax.

$$\begin{aligned}\mu_x &= \text{linspace}(-r_x, r_x, n_j), \\ \mu_y &= \text{linspace}(-r_y, r_y, n_j), \\ \mu_z &= \text{linspace}(-r_z, r_z, n_j),\end{aligned}$$

with $r_x = r_y = r_z = 15$. The event-triggered control update scheme is implemented using a threshold parameter of 0.05. Simulations were performed using MATLAB software for a total duration of 33 time units.

III. Results and Discussions

This section presents the results of the simulation that was done to evaluate the performance of the proposed event-triggered multi-quadrotor formation B-SMC system. The simulation scenario is specifically designed to imitate the main task required to be performed during the inspection of power transmission

cable lines [8]. Specifically, four quadrotor UAVs are tasked to track a cable line segment that is supported by two transmission towers at both ends. The virtual leader is assumed to generate a reference trajectory that starts from the ground point of the first tower. Each quadrotor is required to take off from a predetermined initial position on the ground near the bottom support of the first tower and then fly up to the top of the first tower. After that, each quadrotor then follows along a path defined by the transmission cable that connects the first tower to the second one. Once the cable has been inspected, each quadrotor tracks the second tower from the top until finally landing on the ground near its bottom support.

Figure 4 depicts the three-dimensional (3D) results of the reference trajectory as well as the position trajectories of the four tracker quadrotors. This plot suggests that the resulting quadrotor formation meets the required form of a rectangle shape. In particular, the position tracking errors as shown in Figure 5 suggest

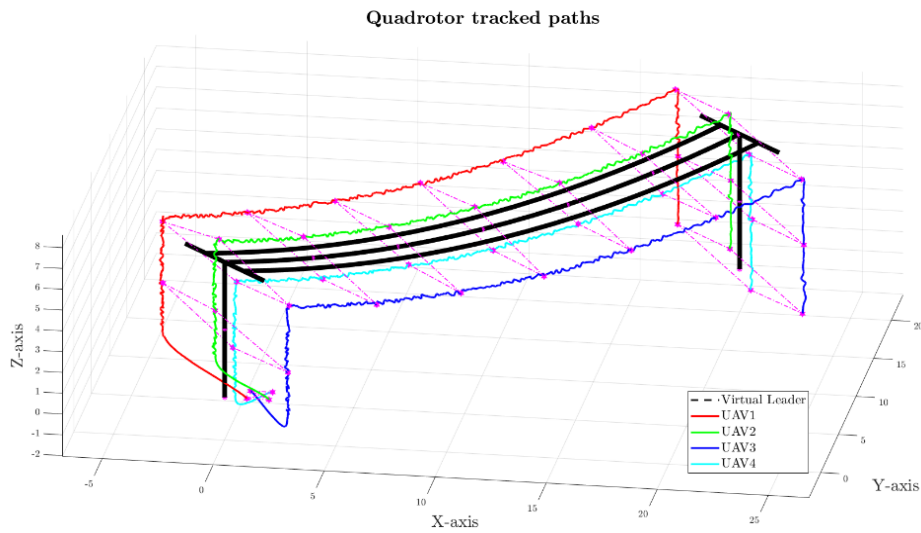


Figure 4. A 3D plot of the simulation tracking simulation result.

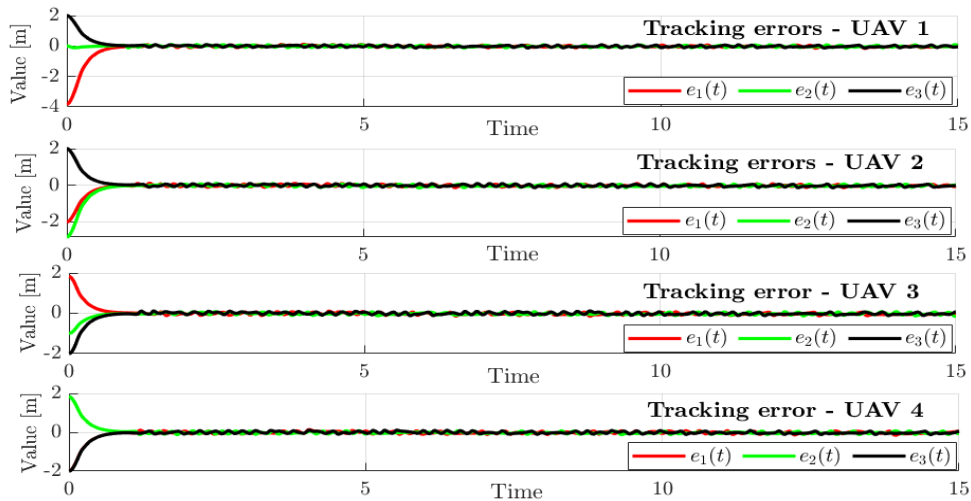


Figure 5. Position tracking errors of each quadrotor.

that each quadrotor satisfactorily tracks the reference position trajectory. These tracking error results were obtained under wind disturbance profiles depicted in Figure 6 with estimates from RBFNN scheme [23] as shown in Figure 7. The proposed event-triggered control implementation successfully maintains the tracking error below the predetermined threshold, which is 0.05 m. However, the disturbance estimations that were produced by the RBFNN are not accurate, as

seen in Figure 7, where the disturbance estimation does not fit the disturbance input graphs on each axis.

Illustrations of the produced event-triggered position control signals for the first quadrotor in the X, Y, and Z axes are shown in Figure 8, Figure 9, and Figure 10, respectively. In the X-axis and Z-axis plots, it can be seen at the beginning of the simulation ($t = 0$) that the event time instances are active, thereby causing the control signal to be updated. However, after a certain time period, the event time instance becomes 0,

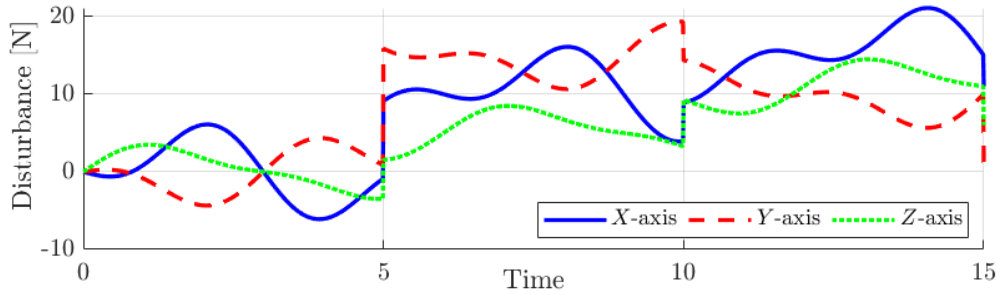


Figure 6. Wind disturbance input for each axis.

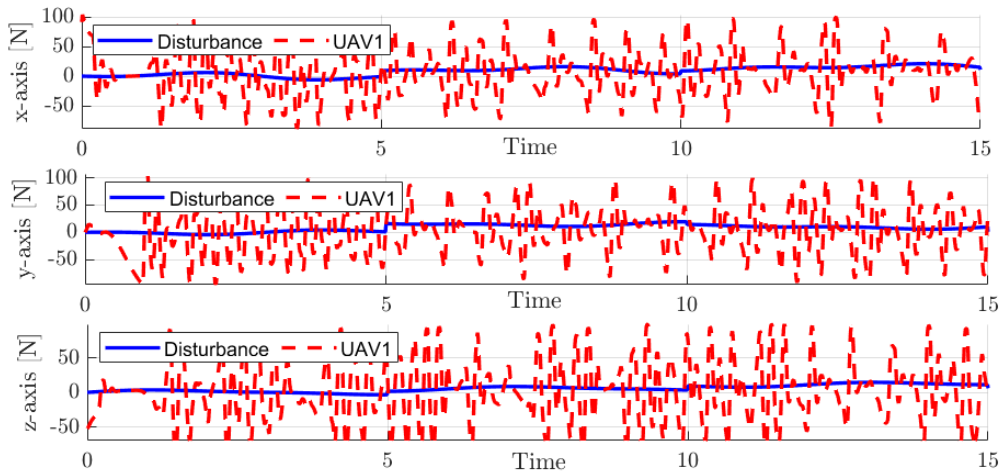


Figure 7. Disturbance estimation for each axis.

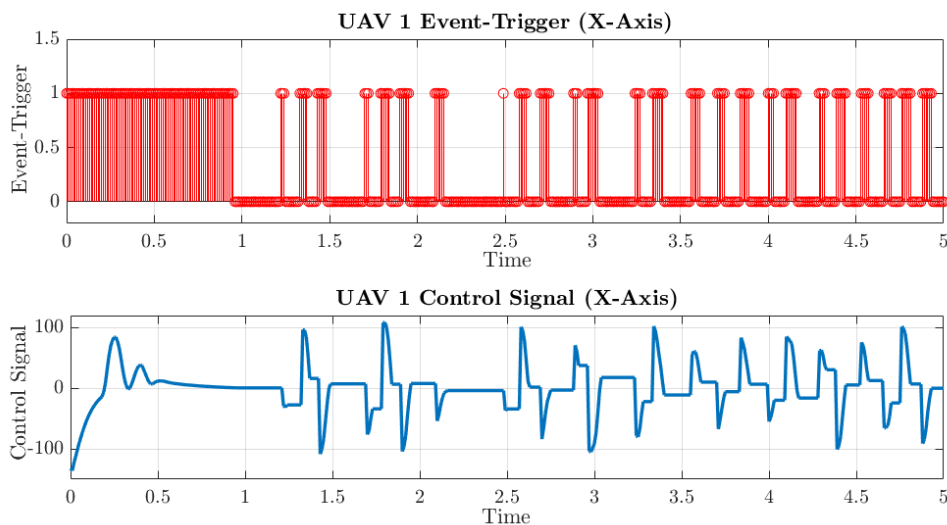


Figure 8. Events and control signals on the X-axis for UAV 1.

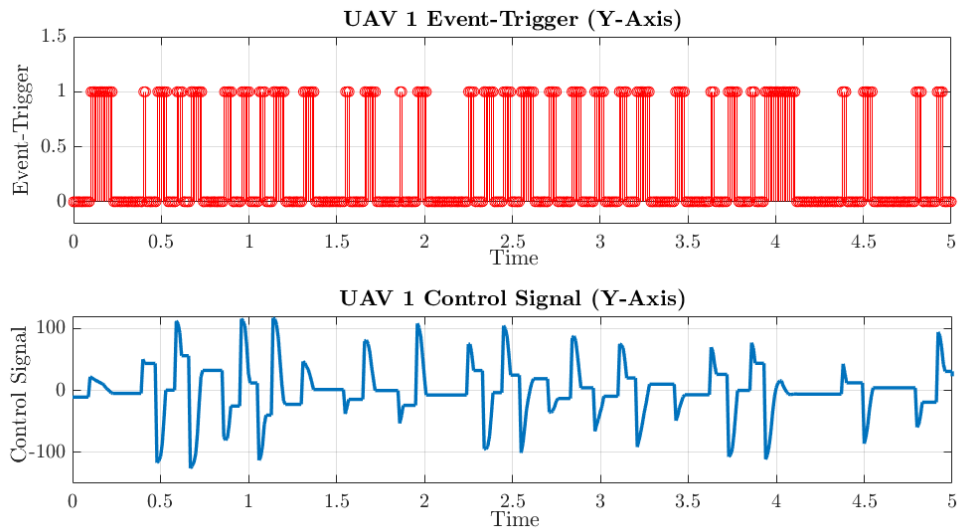


Figure 9. Events and control signals on the Y-axis for UAV 1.

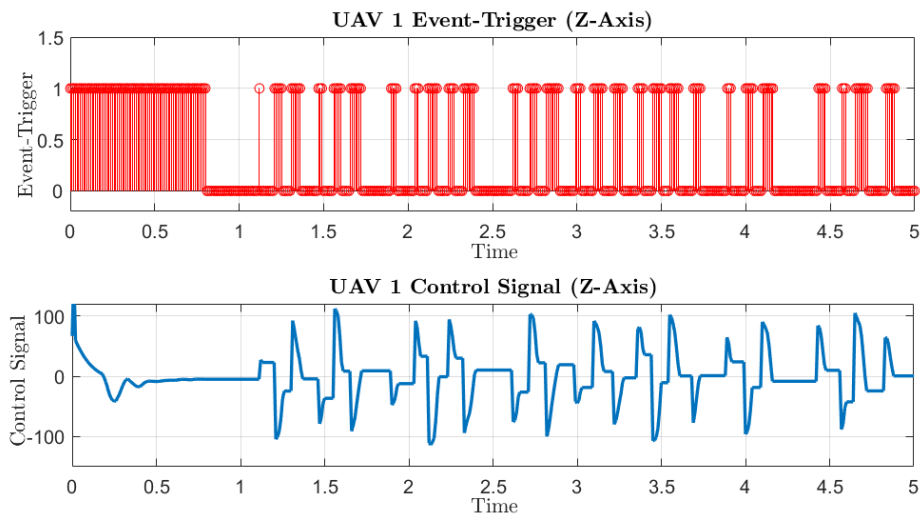


Figure 10. Events and control signals on the Z-axis for UAV 1.

which consequently stops the updates of control signals. This occurs because the event-triggered error signal has crossed the predetermined threshold value [19]. Over the period where the control signal is not updated, the position error increases over time. Once this error magnitude is larger than the threshold value, the event-triggered control will be reactivated and subsequently produce the execution of control signals. For the Y-axis plot, however, it is shown since the beginning of the simulation that the event time instance is inactive. This occurs because the error between the initial position and the desired position from $t = 0$ to $t = 5$ is minimum. Therefore, in this time period, the control signal for the Y-axis is not updated because the error value of the Y-axis is below the predetermined threshold. One important thing to notice in this regard is that the control signals are only produced when necessary, thereby having the potential to efficiently reduce the available computational/communication resources [22].

IV. Conclusion

This paper has presented an event-triggered formation control scheme to manage the operation of multiple quadrotor UAVs in performing the inspection of conventional power transmission lines. In particular, a multi-agent B-SMC method that is equipped with both an RBFNN as an estimator of environmental wind disturbances and an event-triggered control scheme as the control execution framework is proposed to address the required transmission line inspection problem. The presented simulation results illustrate the effective performance of the proposed multi-UAVs control scheme when implemented in a case scenario of tracking conventional transmission cable geometry in the presence of wind disturbance. Simulation results that were presented show that, even with the implementation of event-triggered control the UAVs were able to maintain their desired positions and reach the pre-determined formation. In the event that the

position error of an axis reaches the threshold error of 0.05 m, the control signal was updated to help the UAVs maintain the desired trajectory while minimizing the update of the control signals. Future works can be directed toward implementing the method developed in this paper in real-life experimental tests.

Declarations

Author contribution

T.A. Tamba: Writing – Original Draft, Writing – Review & Editing, Conceptualization, Formal analysis, Investigation, Supervision. **B.C.G. Cinuna:** Writing – Review & Editing, Investigation, Data Curation, Visualization. **Y.Y. Nazaruddin:** Conceptualization, Methodology, Investigation, Validation, Supervision. **M.Z. Romdlony:** Supervision, Resources, Formal Analysis, Data Curation, Visualization, Funding acquisition. **B. Hu:** Investigation, Validation, Writing – Review & Editing.

Funding statement

This research was supported by the Ministry of Education, Culture, Research, and Technology (Kemendikbudristek) of the Republic of Indonesia through the Strategic Research Collaboration (KATALIS) grant scheme year 2024.

Competing interest

The authors declare that they have no known competing financial interests or personal relationships that could have appeared to influence the work reported in this paper.

Additional information

Reprints and permission: information is available at <https://mev.brin.go.id/>.

Publisher's Note: National Research and Innovation Agency (BRIN) remains neutral with regard to jurisdictional claims in published maps and institutional affiliations.

References

- [1] PT. PLN Persero, "Statistics PLN 2023," 2024.
- [2] A. B. Alhassan, X. Zhang, H. Shen, and H. Xu, "Power transmission line inspection robots: A review, trends and challenges for future research," *International Journal of Electrical Power & Energy Systems*, vol. 118, pp. 105862, 2020.
- [3] Y. Luo, X. Yu, D. Yang, and B. Zhou, "A survey of intelligent transmission line inspection based on unmanned aerial vehicle," *Artificial Intelligence Review*, vol. 56, no. 1, pp. 173–201, 2023.
- [4] Z. Wang, Q. Gao, J. Xu, and D. Li, "A review of UAV power line inspection," in *Advances in Guidance, Navigation and Control: Proceedings of 2020 International Conference on Guidance, Navigation and Control, ICGNC 2020, Tianjin, China, October 23–25, 2020*, 2022, pp. 3147–3159.
- [5] C. Xu, Q. Li, Q. Zhou, S. Zhang, D. Yu, and Y. Ma, "Power line-guided automatic electric transmission line inspection system," *IEEE Transactions on Instrumentation and Measurement*, vol. 71, pp. 1–18, 2022.
- [6] X. Li, Z. Li, H. Wang, and W. Li, "Unmanned aerial vehicle for transmission line inspection: status, standardization, and perspectives," *Frontiers in Energy Research*, vol. 9, pp. 713634, 2021.
- [7] M. Chen et al., "Environment perception technologies for power transmission line inspection robots," *Journal of Sensors*, vol. 2021, no. 1, pp. 5559231, 2021.
- [8] S. Kim, D. Kim, S. Jeong, J.-W. Ham, J.-K. Lee, and K.-Y. Oh, "Fault diagnosis of power transmission lines using a UAV-mounted smart inspection system," *IEEE Access*, vol. 8, pp. 149999–150009, 2020.
- [9] M. D. F. Ahmed, J. C. Mohanta, and A. Sanyal, "Inspection and identification of transmission line insulator breakdown based on deep learning using aerial images," *Electric Power Systems Research*, vol. 211, pp. 108199, 2022.
- [10] H. A. Foudeh, P. C.-K. Luk, and J. F. Whidborne, "An advanced unmanned aerial vehicle (UAV) approach via learning-based control for overhead power line monitoring: A comprehensive review," *IEEE Access*, vol. 9, pp. 130410–130433, 2021.
- [11] D.-Q. Chen, X.-H. Guo, P. Huang, and F.-H. Li, "Safety distance analysis of 500kv transmission line tower UAV patrol inspection," *IEEE Letters on Electromagnetic Compatibility Practice and Applications*, vol. 2, no. 4, pp. 124–128, 2020.
- [12] X. Yue, H. Wang, and Y. Jiang, "A novel 110 kV power line inspection robot and its climbing ability analysis," *International Journal of Advanced Robotic Systems*, vol. 14, no. 3, pp. 1729881417710461, 2017.
- [13] L. Yang, J. Fan, Y. Liu, E. Li, J. Peng, and Z. Liang, "A review on state-of-the-art power line inspection techniques," *IEEE Transactions on Instrumentation and Measurement*, vol. 69, no. 12, pp. 9350–9365, 2020.
- [14] Y. Zhang, X. Yuan, Y. Fang, and S. Chen, "UAV low altitude photogrammetry for power line inspection," *ISPRS International Journal of Geo-Information*, vol. 6, no. 1, pp. 14, 2017.
- [15] H. Guan et al., "UAV-lidar aids automatic intelligent powerline inspection," *International Journal of Electrical Power & Energy Systems*, vol. 130, pp. 106987, 2021.
- [16] D. J. Almakhlles, "Robust backstepping sliding mode control for a quadrotor trajectory tracking application," *IEEE Access*, vol. 8, pp. 5515–5525, 2020.
- [17] T. Madani and A. Benallegue, "Backstepping sliding mode control applied to a miniature quadrotor flying

- robot,” in *IECON 2006-32nd Annual Conference on IEEE Industrial Electronics, 2006*, pp. 700–705.
- [18] Z. Jia, J. Yu, Y. Mei, Y. Chen, Y. Shen, and X. Ai, “Integral backstepping sliding mode control for quadrotor helicopter under external uncertain disturbances,” *Aerospace Science and Technology*, vol. 68, pp. 299–307, 2017.
- [19] L. Ding, Q.-L. Han, X. Ge, and X.-M. Zhang, “An overview of recent advances in event-triggered consensus of multiagent systems,” *IEEE Transactions on Cybernetics*, vol. 48, no. 4, pp. 1110–1123, 2018.
- [20] D. V. Dimarogonas, E. Frazzoli, and K. H. Johansson, “Distributed event-triggered control for multi-agent systems,” *IEEE Transactions on Automatic Control*, vol. 57, no. 5, pp. 1291–1297, 2012.
- [21] P. Tabuada, “Event-triggered real-time scheduling of stabilizing control tasks,” *IEEE Transactions on Automatic Control*, vol. 52, no. 9, pp. 1680–1685, 2007.
- [22] X. Shen, J. Gao, and P. X. Liu, “Event-triggered sliding mode neural network controller design for heterogeneous multi-agent systems,” *Sensors*, vol. 23, no. 7, pp. 3477, 2023.
- [23] D.-N. Bui and M. D. Phung, “Radial basis function neural networks for formation control of unmanned aerial vehicles,” *Robotica*, vol. 42, no. 6, pp. 1842–1860, 2024.
- [24] F. Furrer, M. Burri, M. Achtelik, and R. Siegwart, “RotorS—a modular gazebo MAV simulator framework,” *Robot Operating System (ROS): The Complete Reference (Volume 1)*, pp. 595–625, 2016.
- [25] The MathWorks, Inc. (2022). *MATLAB version: 9.13.0 (R2022b)*. Natick, Massachusetts: MathWorks Inc., 2022.